Supporting Information for

The roughness of the protein energy landscape results in anomalous diffusion of the polypeptide backbone

Martin Volk, Lilia Milanesi, Jonathan P. Waltho, Christopher A. Hunter, Godfrey S. Beddard

1. Subdiffusive Behaviour of Polymer Segments in the Rouse and Zimm Models

In the Rouse[1] and Zimm[2] models, polymer dynamics are simulated by approximating the polymer by N beads which are connected to their nearest neighbours by harmonic springs. In the "free-draining" Rouse model, each bead experiences solvent friction independent of the motion of the other beads, whereas the more realistic "non-draining" Zimm model also allows for hydrodynamic interactions between the beads.

The simple Rouse model, using the normally applied "continuous" approximation, which is valid for long polymers, results in relaxation times of the internal modes which are given by[3]

$$\tau_p = \frac{\tau_R}{p^2} \qquad p = 1, 2 \ldots \tag{S1},$$

with the longest relaxation time

$$\tau_R = \frac{fN^2a^2}{3\pi^2 k_B T} \tag{S2},$$

where f is the segmental friction coefficient, a the size of a polymer segment (bead), k_B the Boltzmann constant and T the temperature.

With the Stokes-Einstein relation, $D = k_B T/f$, and values of 10 Å^2/ns for D (*i.e.*, a typical value for the residue diffusion coefficient obtained for unstructured peptides, see main text) and 3.8 Å for a (the C^α-C^α-distance), the longest Rouse relaxation times can be estimated to be on the order of 15 ns for peptides **1** – **3** (N = 17) and 1.5 μs for N-PGK (N = 174).

The Rouse model results in subdiffusive motion of the polymer segments, with their mean square displacement (both in absolute terms and relative to the centre of mass) increasing with time, t, as $\langle r^2(t)\rangle \propto t^{0.5}$ (or $t^{0.54}$, if self-avoidance of the chain is included).[3-7] However, this subdiffusive behaviour is found only for time scales shorter than that for full conformational equilibration, *i.e.* for times shorter than the longest relaxation time τ_R. After this time, the mean square displacement of a polymer segment relative to the centre of mass does not increase further, and its overall motion resembles that of the centre of mass, which follows normal diffusion, $\langle r^2(t)\rangle \propto t$.

It has to be noted that this result is valid strictly only for the "continuous" Rouse model, *i.e.* for very long polymers which have an essentially infinite number of normal modes, and hence an extremely broad relaxation time spectrum, see Eq. (S1). Finite Rouse polymers have a finite number of internal modes and hence a limited relaxation time spectrum whose short-time edge is within the time range relevant here; although rarely investigated in detail, it has been mentioned previously that at times shorter than the shortest relaxation time, segmental motion also is governed by free diffusion.[6,8,9]

For the proteins and peptides investigated here, consisting of only 17 residues (peptides **1**-**3**) or 174 residues (N-PGK), the continuous approximation is not justified any more. In the following, we show how the limited number of normal modes modifies the diffusional behaviour of polymer segments in such short polypeptides, using the finite (discrete) Rouse model,[1,7,10] which – unlike the standard implementation of the Rouse model[3] – does not use the simplifications achieved by assuming a continuous polymer backbone, but fully takes into account the limited number of internal modes.

The finite Rouse model yields relaxation times for the (N-1) internal modes which are slightly different to those obtained from the continuous Rouse model:[1,10]

$$\tau_p = \tau_R \frac{(\pi/2N)^2}{\sin^2(p\pi/2N)} \qquad p = 1, 2 \ldots (N-1) \qquad \text{(S3)},$$

with τ_R given by Eq. (S2); note that these relaxation times are the same as those for the continuous Rouse model, Eq. (S1), for p << N, whereas for p → N, *i.e.* for the fast relaxing modes, the discrete Rouse model yields relaxation times which are larger by a factor of $(\pi/2)^2 = 2.5$.

The mean square displacement of the nth segment in the discrete Rouse model is given by:[7]

$$< r_n^2(t) > = \frac{2Na^2}{\pi^2}\frac{t}{\tau_R} + \frac{a^2}{N}\sum_{p=1}^{N-1}\cos^2\left(\frac{p\pi(n-1/2)}{N}\right)\left(1 - e^{-t/\tau_p}\right) \qquad \text{(S4)}$$

In Eq. (S4), the first term describes the centre of mass motion of the full polymer and the second term the internal motion of segment n relative to the centre of mass.

Fig. S1 shows the mean square displacement of segments in the centre and at the ends of a polymer calculated from Eq. (S4) for polymers with 17 beads (corresponding to peptides **1** – **3**) and 174 beads (comparable to fully unfolded N-PGK), respectively. For better comparability, these are shown on normalised time and length scales (normalised to τ_R and a, respectively). These simulations confirm that subdiffusive behaviour of polymer segments, $<r^2(t)> \propto t^{0.5}$, also is observed in the finite Rouse model. However, subdiffusive behaviour is limited to the time scale between the shortest and the longest Rouse relaxation time given by Eq. (S3). At shorter times, polymer segments follow normal diffusion, whereas at longer times the mean square displacement of residues with respect to each other does not change any further, since full relaxation between all polymer conformations has taken place.

The actual ranges of Rouse relaxation times can be estimated to be around 130 ps - 15 ns for peptides **1** – **3** ($N = 17$) and 120 ps – 1.5 μs for N-PGK ($N = 174$), respectively, from the values of τ_R given above and Eq. (S3). Due to their limited polymer lengths, subdiffusive behaviour is expected to extend over not more than two orders of magnitude in time for peptides **1** – **3** and not more than four orders of magnitude for N-PGK. It should be noted that here we have assumed that each polypeptide residue corresponds to one Rouse bead, which is not quite correct since chain stiffness effects lead to neighbouring residues not being completely independent of each other. Thus, a somewhat smaller number of Rouse beads, and hence an even narrower relaxation time spectrum, could be expected. The inclusion of internal friction, which recently has been highlighted to be of significant importance for the dynamics of unfolded polypeptides, see main text, is expected to further reduce the (relative) width of the relaxation time spectrum of the Rouse model, particularly for relatively short polymers, such as the ones discussed here.[11,12] It also should be noted that the N-PGK residues to which the thiyl radicals are tethered are separated by only 11 residues, so that their relative diffusion is expected to lead to equilibration on a significantly shorter time scale than that estimated from the Rouse relaxation time of the whole polypeptide.[12,13]

The more realistic Zimm model also results in subdiffusive behaviour, although motion is not as strongly subdiffusive as that expected for the Rouse model ($<r^2(t)> \propto t^{0.67}$).[14] Furthermore, the Zimm model has a weaker dependence of the relaxation times on the mode number:

$$\tau_p = \frac{\tau_1}{p^{1.5}} \qquad p = 1 \ldots (N-1) \qquad \text{(S5)},$$

with the longest relaxation time given by

$$\tau_1 = 0.325\frac{\eta_S N^{1.5} a^3}{k_B T} \qquad \text{(S6)},$$

where η_S is the viscosity of the solvent.[3] This weaker power dependence on the mode number results in a narrower relaxation time spectrum; *e.g.*, for a polymer with 174 beads, the ratio of the longest to

the shortest relaxation time in the finite Rouse model is ~12,000, whereas for the Zimm model, the ratio is only ~2,300. To the best of our knowledge, there is no theoretical treatment of the segmental mean square displacements in a finite Zimm polymer, but it is expected that this narrower relaxation time spectrum will result in a correspondingly narrower time range over which subdiffusive motion occurs.

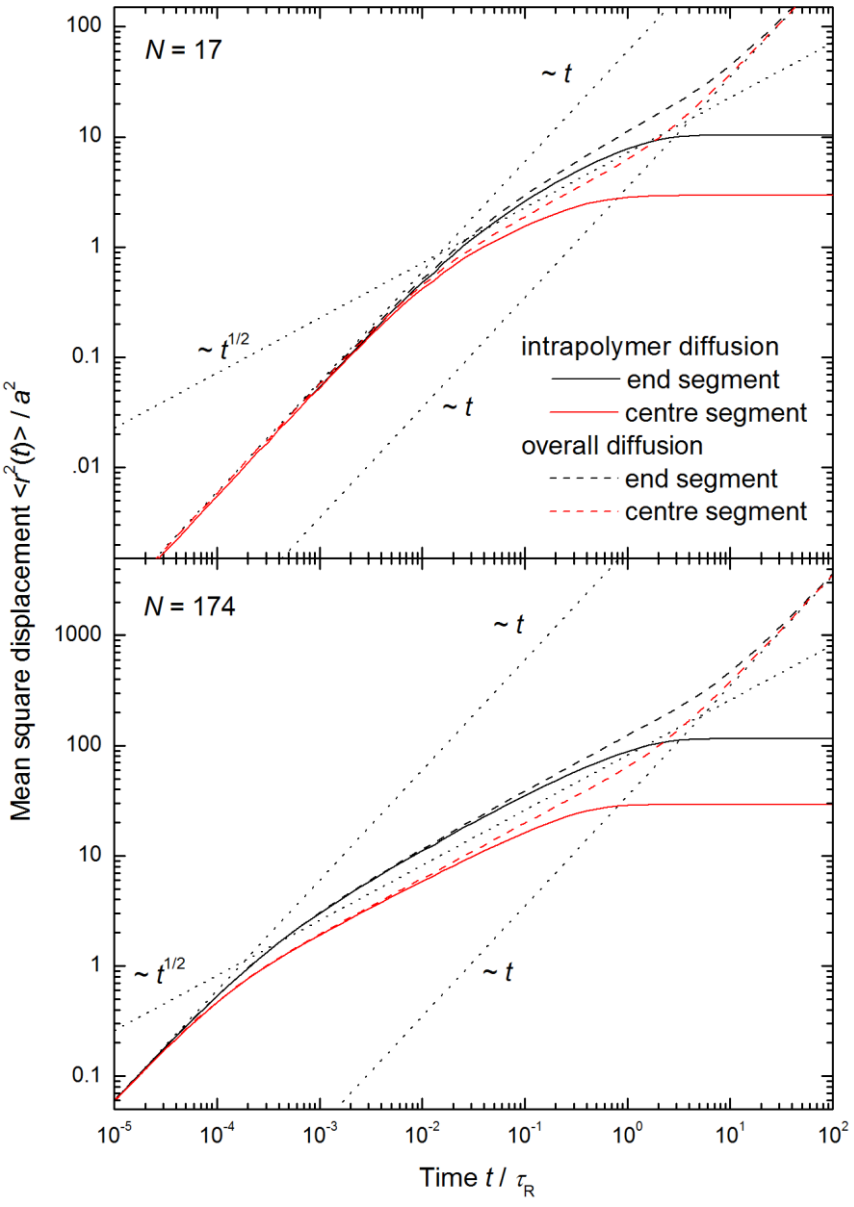

Fig. S1 Time dependence of the mean square displacement $\langle r^2(t) \rangle$ of a polymer segment, normalised to the segment size, a, calculated from the finite Rouse model, Eq. (S4). Shown are the results for the overall displacement (dashed lines) and for diffusion relative to the centre of mass (solid lines) for a polymer with 17 residues (top) and for a polymer with 174 residues (bottom). The time axis is normalised to the maximum Rouse time, τ_R, Eq. (S2)

2. Random Walk Simulations Comparing Normal and Subdiffusive Motion

For a direct comparison of the behaviour of peptide segments undergoing normal and subdiffusive motion, we performed a series of random walk simulations, focussing on the time dependence of the mean square displacement, $\langle r^2(t)\rangle$, as well as the distribution of the displacements obtained after different times. These simulations confirm that a subdiffusively moving particle spends a larger fraction of time close to its initial position than a particle undergoing normal diffusion,[15,16] which for (tethered) polypeptide segments leads to significantly slower equilibration over the accessible space. They also confirm quantitatively that it is reasonable to suggest that in the case of strong subdiffusion no full equilibration over all polypeptide conformations is achieved within the experimental time scale of the experiments shown in Figs. 4 and 5 (1 ms).

The random-walk simulations employed here follow a non-reacting free (unbound) particle which starts at the origin at $t = 0$ and moves on a three-dimensional cubic lattice with a spacing b between neighbouring sites. For normal diffusion, each site is assumed to have the same jump rate $\gamma = \gamma_r$. For simulating subdiffusion caused by inhomogeneous trapping, upon arrival at a site a trap energy E is randomly taken from an exponential distribution

$$g(E) = \frac{\alpha}{k_B T} e^{-\frac{\alpha E}{k_B T}} \qquad \text{(S7)},$$

where α corresponds to the subdiffusive parameter, k_B is the Boltzmann constant and T the temperature; a site with trap energy E is assumed to have a reduced (activated) jump rate

$$\gamma(E) = \gamma_r e^{-\frac{E}{k_B T}} \qquad \text{(S8)}$$

After arriving at a site, a jump to a randomly chosen neighbouring sites takes place after a waiting time t_{wait} which is determined randomly from an exponential distribution with an average value $1/\gamma_r$ or $1/\gamma(E)$, respectively. This approach has been used previously for modelling subdiffusive motion due to inhomogeneous trapping[17] and corresponds to the assumptions made in the simulations of subdiffusive geminate recombination shown in Fig. 7.[18] As has been reported previously,[17] and is confirmed in Fig. S2, the random distribution $g(E)$ given in Eq. (S7) yields subdiffusive behaviour, $\langle r^2(t)\rangle \sim t^{\alpha}$.

The numerical value for the free (or non-activated) diffusion jump rate, γ_r, was assumed to correspond to the Eyring frequency factor $k_B T/h = 6.2\ 10^{12}\ s^{-1}$, where h is Planck's constant. The jump distance b was adjusted so that normal diffusion with a diffusion constant $D = 4$ Å^2/ns is obtained, yielding a reasonable value of $b = 0.062$ Å.[†]

Fig. S2 shows some of the results obtained from averaging over 1×10^4 (free diffusion) or 5×10^6 runs (subdiffusion). For free diffusion, the theoretically predicted time dependence, $\langle r^2(t)\rangle = 6Dt$, is found (Fig. S2 top), and the distribution of displacements at all times is given by a Gaussian radial distribution (in three dimensions), $P(r) \sim r^2 \exp(-r^2/4Dt)$ (Fig. S2, bottom left). These results confirm that polypeptide segments undergoing normal diffusion with D ~ 4 Å^2/ns are expected to diffuse over a length scale comparable to the equilibrium distance between the thiol binding sites (35-45 Å, see main text; this region is indicated by the hatched area in Fig. S2, top) on the 10-100 ns time scale, so that full equilibrium between all conformations could be expected on this time scale.

In contrast, much slower motion is found upon introducing traps with a distribution of trap energies, if those include a significant number of traps which are deeper than thermal energies (small α). Fig. 2

[†] Simulations with different values of γ_r yield identical results for free diffusion if the value of b is adjusted in the same manner, but yield faster or slower subdiffusive motion if γ_r is decreased or increased, respectively. However, even for an unrealistically low jump attempt rate, γ_r, of $2\times10^9\ s^{-1}$ (corresponding to a jump size of 3.5 Å, *i.e.* the full size of a single residue), subdiffusive motion with $\alpha = 0.3$ leads to an average displacement of only 30 Å after 1 ms. Thus, even for these parameters, the main conclusion, namely that subdiffusive motion prevents full equilibration over all polypeptide conformations within the experimental time scale, is still valid.

(top) confirms that $\langle r^2(t)\rangle \sim t^{\alpha}$ for the trap energy distribution given by Eq. (S7). The distribution of displacements is quite different to that expected for free diffusion and cannot be fitted by a Gaussian distribution, see Fig. S2 (bottom right), in agreement with theoretical predictions.[15,19] Most importantly, even after 1 ms, diffusion has only occurred on the length scale of a few Å, and thus has not progressed sufficiently to cause full equilibration over all conformations, which requires diffusion over a length scale given by the equilibrium distance between the thiol binding sites (35-45 Å).

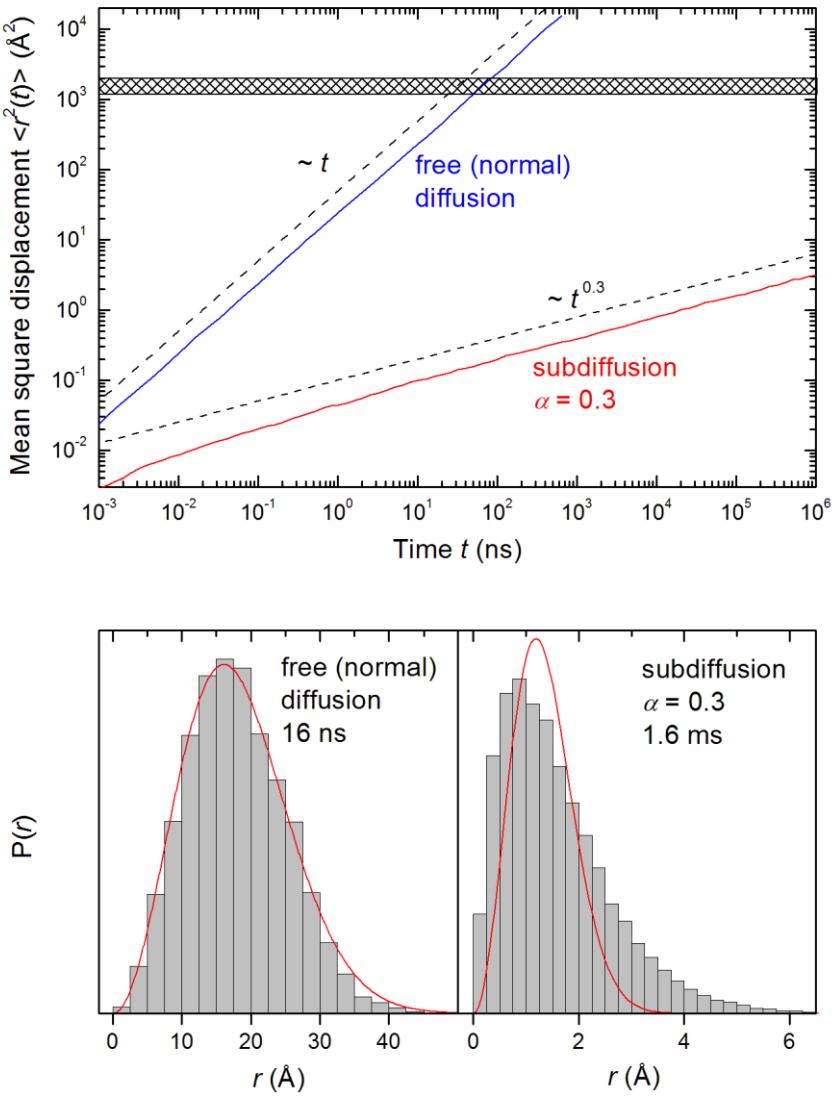

Fig. S2 Results of random-walk simulations of a particle following normal or subdiffusive motion. Shown are the time dependence of the mean square displacement $\langle r^2(t)\rangle$ of a particle (top; normal diffusion, blue, and subdiffusive motion with $\alpha = 0.3$, red; the hatched area indicates the region where $\langle r^2(t)\rangle$ is between (35 Å)^2 and (45 Å)^2) and the distribution of distances over which the particle has moved in different runs after 16 ns (normal diffusion) or 1.6 ms (subdiffusion with $\alpha = 0.3$), respectively (bottom). Values of $\gamma_r = k_B T/h$ and $b = 0.062$ Å were assumed, yielding a normal diffusion constant D = 4 Å^2/ns, see text. The red lines in the bottom panels are the best fits to a Gaussian radial distribution of distances, $P(r) \sim r^2 \exp(-r^2/\sigma^2)$, with σ as a free fit parameter; for free diffusion (left panel), σ^2 is found to correspond to $4Dt$.

3. Inhomogeneous Trap Model of Geminate Recombination

In our experiments, we are observing the geminate recombination of thiyl radical pairs after disulfide bond photolysis and calculate the instantaneous rate constant

$$k_{\mathrm{inst}}(t) = -\frac{\mathrm{d}c(t)/\mathrm{d}t}{c(t)} = -\frac{\mathrm{d}A(t)/\mathrm{d}t}{A(t)} \qquad \text{(S9)},$$

where t is the time after photolysis and $c(t)$ is the surviving radical concentration, which is directly reflected in the measured transient absorbance $A(t)$.

We find an unusual power law for $k_{\mathrm{inst}}(t) \sim t^{-0.94}$ over nine orders of magnitude in time, from pico- to milliseconds, Fig. 5 of the main text. The wide range of rate constants observed in these experiments is a consequence of the various interactions caused by van-der-Waals interactions, π-π stacking, hydrogen bonds and salt bridges etc. between the various amino acids of the partly folded and unfolded protein, as well as other effects, such as dihedral rotational energies or the energetic cost of creating voids. Calculations and experiments on several proteins indicate that the magnitude of van-der-Waals interactions,[20] π-π stacking[21] and aromatic/hydrophobic effects,[22] hydrogen bonds[23] or salt bridges[24] is frequently of the order of at most a few $k_{\mathrm{B}}T$. This relatively small energy is controlled largely by the geometric constraints placed upon residues when a folded protein is in its native state. In a peptide chain or unfolded or partly folded protein, there is the possibility that this energy could be larger because the geometric constraints are not so severe and the molecules can approach one another in a more favourable way. Additionally, there is the possibility that several separate interactions can be present. With this in mind, we find that a simple kinetic model does describe the variation of $k_{\mathrm{inst}}(t)$ vs. time surprisingly well.

In this simple model, we assume that the radicals become trapped in close vicinity of each other immediately after bond photolysis and recombine directly upon escape from this trap. Trapping of the radicals occurs because the backbone becomes trapped in a local minimum of the rough energy landscape which is caused by the interactions just described. Escape from the trap thus has an activation energy that must be overcome before S - S recombination can occur. The rate constant for breaking the intermolecular interaction is described by the Arrhenius type equation

$$k_n = k_0 \exp\left(-E_n / k_B T\right) \qquad \text{(S10)},$$

where E_n is the energy of the n^{th} interaction and k_0 the maximum rate constant. Because of this exponential relationship, a relatively small range of E_n will lead to a huge variation in k_n or, which is the same, a huge range of lifetimes over which the interaction between residues persists. Thus, if $k_0 = 10^{12}\ \mathrm{s}^{-1}$ (*i.e.* just slightly smaller than the maximum value predicted by Eyring theory), a change of E_n from 0 to 60 kJ/mol (~25 $k_{\mathrm{B}}T$ at room temperature) causes the lifetime of the interaction to change from 1 ps to ~4 ms. Therefore, motions like internal restricted rotation around single bonds with very small activation barriers will be responsible for the picosecond time scale behaviour, whereas the combined action of several interactions such as hydrogen bonds is required to trap a backbone conformation on the millisecond range.

The probability that the n^{th} interaction (with activation energy E_n) lasts up to time t is

$$p_n(t) = e^{-k_n t} \qquad \text{(S11)}$$

Since there are different interaction energies, there will naturally be a distribution in their number. Because we do not know *a priori* what this will be, by appealing to the Central Limit Theorem of statistics it seems reasonable to let this be a Gaussian with a most likely energy E_0, variance σ_{E}^2 and normalisation constant N,

$$G_n = N \exp\left(-\frac{(E_n - E_0)^2}{2\sigma_{\mathrm{E}}{}^2}\right) \qquad \text{(S12)}$$

When $E_0 \to 0$, the largest number of interactions occurs for small energies, and their number decreases as their energy increases, which is what one expects for the hierarchical protein energy

landscape. A similar model has been used recently for describing the motion of "sticky" particles over a surface, which is highly subdiffusive due to a wide distribution of traps.[25]

The cumulative probability that interactions last up to time t thus gives the time-dependent concentration of surviving radicals:

$$c(t) = \sum_n p_n(t) G_n = \int p_n(t) G_n dE_n \tag{S13}$$

where the sum is over all interactions and can be replaced by an integral due to the large number of potential trap depths; strictly speaking, summation/integration should only be performed to a value E_{max}, corresponding to the maximum trap depth, which must be finite in a real system. However, this will only affect the dynamics at times outside the window of interest here, as long as $E_{max} > 25\ k_B T$, see above and also compare the discussion of maximum trap depths and equilibration in the main text.

This yields the following expression for the instantaneous rate constant:

$$k_{inst}(t) = -\frac{1}{c}\frac{dc}{dt} = \sum_n k_n p_n(t) G_n \Big/ \sum_n p_n(t) G_n = \int k_n p_n(t) G_n dE_n \Big/ \int p_n(t) G_n dE_n \tag{S14}$$

Fig. S3 shows results for $k_{inst}(t)$ obtained with this model. Most notably, for a distribution of trap depths with significant width (i.e. $\sigma_E \geq 5\ k_B T$), $k_{inst}(t)$ is found to follow a power law which closely resembles the experimental result $k_{inst}(t) \sim t^{-0.94}$ over the whole time range of the experiment (1 ps - 1 ms). This is more clearly shown in Fig. 8B, which presents the results of power law fits to the simulations on different time scales for trap depth distributions of different widths. For $\sigma_E \geq 5\ k_B T$, the power law found over the whole time range is very close to $k_{inst}(t) \sim t^{-0.94}$.

It should be noted that the deviations from this power law at shorter times, which are most pronounced for narrow trap depth distributions, arise from the fact that the rate constant for trap escape has a maximum value k_0 and $k_{inst}(t)$ obviously cannot exceed this value. The effect of this capping can be clearly seen by comparing the simulations for different values of k_0 in Fig. S3 (solid and dashed lines). On the other hand, the larger value used there, $k_0 = 6\ ps^{-1}$ is very close to the prefactor $k_B T/h$ in the Eyring equation, so it does not seem sensible to assume an even larger value, indicating that a trap depth distribution with a width of at least several $k_B T$ is required to rationalise the experimental observation that the power law behaviour of $k_{inst}(t)$ persists down to this short time scale.

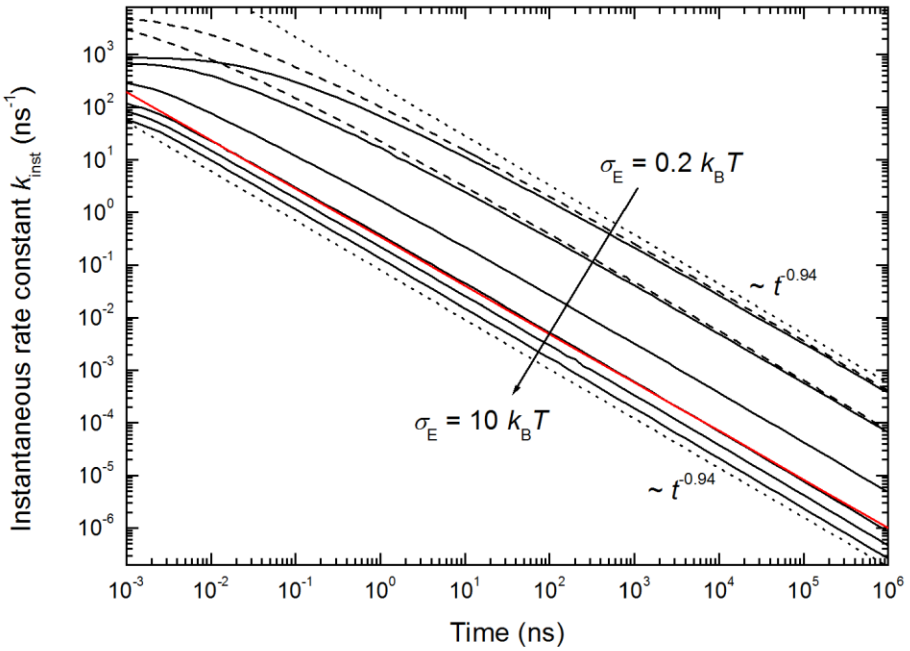

Fig. S3 Time dependence of the instantaneous rate constant $k_{inst}(t)$, simulated with the simplified model of a single trapping site with a distribution of trap depths described here. Parameters: (solid lines) $k_0 = 1$ ps^{-1}, $E_0 = 0$, $\sigma_E/k_BT = 0.2, 0.5, 2, 5, 7, 10$; (dashed lines) $k_0 = 6$ ps^{-1}, $E_0 = 0$, $\sigma_E/k_BT = 0.2, 0.5$. The dotted lines show the power law ~ t$^{-0.94}$ and the solid red line is a power law fit to the full curve for $\sigma_E = 5\ k_BT$, yielding a power law ~ t$^{-0.92}$.

References

1 P. R. Rouse, *J. Chem. Phys.*, 1953, **21**, 1272-1280.
2 B. H. Zimm, *J. Chem. Phys.*, 1956, **24**, 269-278.
3 M. Doi and S. F. Edwards, *The Theory of Polymer Dynamics*, Clarendon Press, Oxford, 1986
4 P. G. deGennes, *Physics*, 1967, **3**, 37-45.
5 A. Baumgärtner, *J. Chem. Phys.*, 1980, **72**, 871-879.
6 G. S. Grest and K. Kremer, *Phys. Rev. A*, 1986, **33**, 3628-3631.
7 V. A. Harmandaris, V. G. Mavrantzas, D. N. Theodorou, M. Kröger, J. Ramirez, H. C. Öttinger and D. Vlassopoulos, *Macromolecules*, 2003, **36**, 1376-1387.
8 K. Kremer, *Macromolecules*, 1983, **16**, 1632-1638.
9 K. Kremer and K. Binder, *J. Chem. Phys.*, 1984, **81**, 6381-6394.
10 P. H. Verdier, *J. Chem. Phys.*, 1966, **45**, 2118-2121.
11 B. S. Khatri and T. C. B. McLeish, *Macromolecules*, 2007, **40**, 6770-6777.
12 A. Soranno, B. Buchli, D. Nettels, R. R. Cheng, S. Mueller-Spaeth, S. H. Pfeil, A. Hoffmann, E. A. Lipman, D. E. Makarov and B. Schuler, *Proc. Natl. Acad. Sci. U.S.A.*, 2012, **109**, 17800-17806.
13 D. E. Makarov, *J. Chem. Phys.*, 2010, **132**, 035104.
14 R. Shusterman, S. Alon, T. Gavrinyov and O. Krichevsky, *Phys. Rev. Lett.*, 2004, **92**, 048303.
15 R. Metzler and J. Klafter, *Phys. Rep.*, 2000, **339**, 1-77.
16 G. Guigas and M. Weiss, *Biophys. J.*, 2008, **94**, 90-94.
17 K. Seki, M. Wojcik and M. Tachiya, *J. Chem. Phys.*, 2003, **119**, 7525-7533.
18 L. Milanesi, J. P. Waltho, C. A. Hunter, D. J. Shaw, G. S. Beddard, G. D. Reid, S. Dev and M. Volk, *Proc. Natl. Acad. Sci. U.S.A.*, 2012, **109**, 19563-19568.
19 J. A. Dix and A. S. Verkman, *Annu. Rev. Biophys.*, 2008, **37**, 247-263.
20 J. Caillet and P. Claverie, *Acta Crystallogr., Sect. A*, 1975, **31**, 448-461.
21 C. A. Hunter and J. K. M. Sanders, *J. Am. Chem. Soc.*, 1990, **112**, 5525-5534.
22 L. Serrano, M. Bycroft and A. R. Fersht, *J. Mol. Biol.*, 1991, **218**, 465-475.
23 A. R. Fersht, *Trends Biochem. Sci.*, 1987, **12**, 301-304.
24 A. Horovitz, L. Serrano, B. Avron, M. Bycroft and A. R. Fersht, *J. Mol. Biol.*, 1990, **216**, 1031-1044.
25 Q. Xu, L. Feng, R. Sha, N. C. Seeman and P. M. Chaikin, *Phys. Rev. Lett.*, 2011, **106**, 228102.